Design of microresonators to minimize thermal noise below the standard quantum limit

S. Sharifi [iD], Y. M. Banadaki, T. Cullen, G. Veronis, J. P. Dowling, and T. Corbitt

View Online　　　**Export Citation**　　　**CrossMark**

Design of microresonators to minimize thermal noise below the standard quantum limit

View Online   Export Citation   CrossMark

S. Sharifi,[1,2,3,4,a] (iD) Y. M. Banadaki,[4,5] T. Cullen,[1] G. Veronis,[2,3] J. P. Dowling,[1,4] and T. Corbitt[1,4]

AFFILIATIONS

[1] Department of Physics and Astronomy, Louisiana State University, Baton Rouge, Louisiana 70803, USA
[2] School of Electrical Engineering, Louisiana State University, Baton Rouge, Louisiana 70803, USA
[3] Center for Computation and Technology, Louisiana State University, Baton Rouge, Louisiana 70808, USA
[4] Hearne Institute for Theoretical Physics, Louisiana State University, Baton Rouge, Louisiana 70803, USA
[5] Department of Computer Science, Southern University, Baton Rouge, Louisiana 70813, USA

[a] Author to whom correspondence should be addressed: sshari2@lsu.edu

ABSTRACT

Microfabricated resonators play a crucial role in the development of quantum measurement, including future gravitational wave detectors. We use a micro-genetic algorithm and a finite element method to design a microresonator whose geometry is optimized to maximize the sub-Standard Quantum Limit (SQL) performance including lower thermal noise (TN) below the SQL, a broader sub-SQL region, and a sub-SQL region at lower frequencies. For the proposed design, we study the effects of different geometries of the mirror pad and cantilever microresonator on sub-SQL performance. We find that the maximum ratio of SQL to TN is increased, its frequency is decreased, and the sub-SQL range is increased by increasing the length of the microresonator cantilever, increasing the radius of the mirror pad, decreasing the width of the microresonator cantilever, and shifting the laser beam location from the mirror center. We also find that there exists a trade-off between the maximum ratio of SQL to TN and the sub-SQL bandwidth. The performance of this designed microresonator will allow it to serve as a test-bed for quantum non-demolition measurements and to open new regimes of precision measurement that are relevant for many practical sensing applications, including advanced gravitational wave detectors.

I. INTRODUCTION

One hundred years after Albert Einstein predicted the existence of gravitational waves in his general theory of relativity,[1] the Laser Interferometer Gravitational-Wave Observatory (LIGO)[2] and advanced Virgo[3] have opened a new window to the universe by detecting the first gravitational waves in 2015.[4] These discoveries impel the need to develop strategies for improving the rate of detections by decreasing the limiting noise sources in gravitational wave interferometers.[5–8] Quantum mechanics dictates that the precision of physical measurements is subjected to certain constraints. The Standard Quantum Limit (SQL) sets a limit for conventional continuous interferometric displacement measurements. The SQL balances the imprecision of the measurement from photon statistics with the unwanted quantum back action (radiation pressure noise). Pushing the displacement measurements toward this limit is crucial for improving systems ranging from nanomechanical devices,[9] ultracold atoms,[10] and Advanced LIGO.[11] To go beyond the SQL, correlations between shot noise and radiation pressure noise must be created. Various techniques have been proposed to achieve this, including speed-meter interferometers,[12] which monitor the relative momentum of the test-mass mirrors, and using optical springs,[13] which manifest as a restoring force created by the optical field. Recently, Mason *et al.*[14] exploited strong quantum correlations in an ultra-coherent optomechanical system and demonstrated off-resonant force and displacement sensitivity reaching 1.5 dB below the SQL. Yu *et al.*[15] proved that the SQL can be surpassed via correlations within the position/momentum uncertainty of the object and the photon number/phase uncertainty of the light it reflects.

Quantum noise, including quantum radiation pressure noise (QRPN),[16] is one of the main limiting phenomena across a wide

range of frequencies that originate from the quantum nature of photons in an interferometer. However, classical noise sources such as environmental vibrations and thermally driven fluctuations are typically large and can prevent sub-SQL measurements. Approaching sub-SQL measurements in optomechanical systems has relied on techniques[17–19] aiming at first reducing the thermal motion and then testing the proposals for reducing QRPN.[20–26] The non-negligible thermal noise (TN), which is governed by the fluctuation-dissipation theorem,[27] sets a limit on the motion of mechanical resonators.[28]

In a recent paper,[29] we presented a broadband and off-resonance measurement of QRPN in the audio frequency band. We developed low-loss single-crystal microresonators with sufficiently minimized thermal noise, so that the QRPN was observed at room temperature. The noise spectrum obtained showed effects due to QRPN between about 2 kHz and 100 kHz. In this paper, we use a micro-genetic algorithm and a finite element method (FEM) based model to design new GaAs/AlGaAs microresonators, to study the effects of different geometries of the mirror pad and cantilever microresonator and to minimize TN well below the SQL. The new microresonators will enable broadband, off-resonance sub-SQL experiments and serve as a test-bed for sub-SQL and back action evasion techniques. In addition, this optomechanical device can operate as a filter cavity inside the signal-recycling cavity in the unstable regime.[30] The unstable filter acts as a phase compensator with negative dispersion in the single loop where a feedback control stabilizes the entire system. Within the loop, free propagation inside the arm cavity causes phase lag of the sidebands that can be compensated by the unstable filter. Minimizing the thermal noise of the unstable microresonator filters enables the implementation of this scheme and enhances the bandwidth of advanced gravitational wave detectors.

This paper is organized as follows: In Sec. II, we describe the theory of designing the new microresonators using the micro-genetic algorithm and the model equations of TN and SQL that are used to evaluate the measurement of the new microresonators at the sub-SQL regime. This section is followed by a discussion of the effect of changing the geometry of the mirror pad and microresonator cantilever on the sub-SQL region of displacement measurement. Finally, our conclusions are summarized in Sec. IV.

II. DESIGN OF NEW MICRORESONATORS

Figure 1 shows the optomechanical system consisting of a Fabry–Pérot cavity with a mechanical oscillator as one of the cavity mirrors. The optomechanical cavity has a high-reflectivity, single-crystal microresonator that serves as the input coupler and a half-inch diameter mirror as the back reflector. A Nd:YAG laser beam is used to both stabilize the optomechanical cavity and measure the mechanical motion of the microresonator. The cavity is locked using a feedback loop that utilizes the restoring force produced by a strong optical spring.[31] The details of the optomechanical system can be found in Ref. 31. Here, we focus on designing a new microresonator and on studying the effect of varying its geometry on the sub-SQL region. While the mirrors currently used in gravitational wave detectors are based on silica/tantala coatings,[32,33] GaAs/AlGaAs crystalline coatings experimentally show great promise for reducing Brownian coating thermal noise[34–36] and are, therefore, being considered as coatings for the next-generation gravitational wave detectors.

Figures 2(a) and 2(b) show schematics of the cross sections of the microresonator mirror pad structures that are designed from alternating layers of GaAs and $Al_{0.92}Ga_{0.08}$, as in Ref. 29 and as in this paper, respectively. A multilayer stack of alternate GaAs and $Al_{0.92}Ga_{0.08}As$ thin films used as high and low index materials forms a Fabry–Pérot cavity or Bragg mirrors.[37] The mirror pad in Fig. 2(a) includes 23 pairs of GaAs and $Al_{0.92}Ga_{0.08}As$, one thick layer of GaAs (133.8 nm), and two thick layers of GaAs and
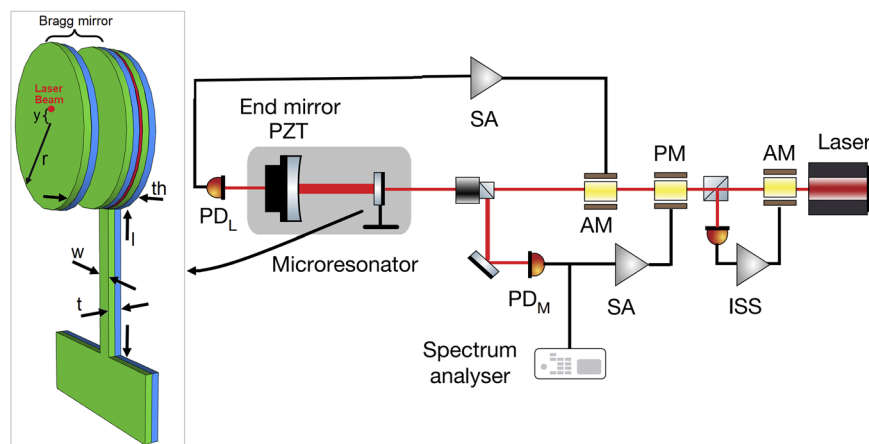

FIG. 1. Experimental arrangement of our optomechanical system. The optomechanical cavity consists of a macroscopic end mirror and a microresonator.[31] The mirror pad consists of multiple layers of GaAs/$Al_{0.92}Ga_{0.08}$ quarter-wave optical pairs in a Bragg mirror, an InGaP buffer layer, and a GaAs/$Al_{0.92}Ga_{0.08}As$ pair that also holds the cantilever microresonator. The geometric parameters of the microresonator are the mirror pad radius (r), its thickness (th), the distance of the laser beam spot from the mirror pad center (y), and the microresonator cantilever length (l), width (w), and thickness (t). Reproduced with permission from Cripe et al., Phys. Rev. A **97**, 013827 (2018). Copyright 2018 American Physical Society.
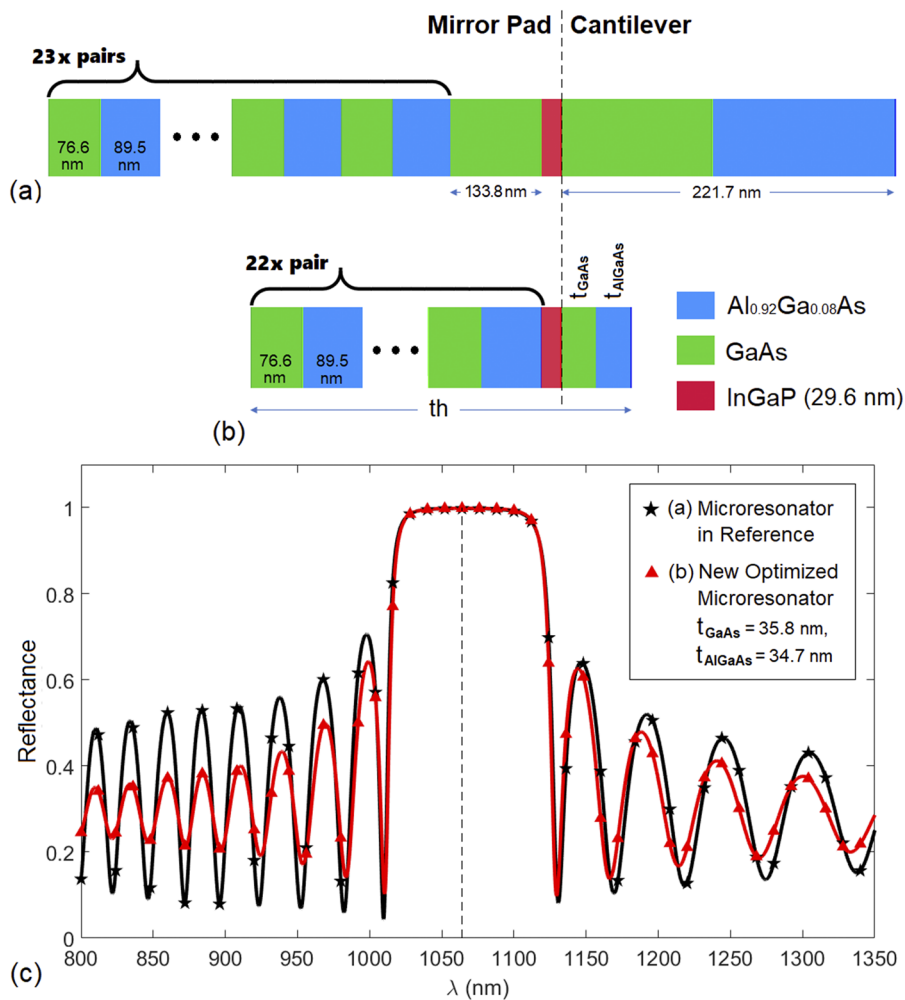
FIG. 2. Cross-sectional schematic of (a) the microresonator mirror pad design in Ref. 29 and (b) microresonator mirror pads designed using our optimization algorithm.[46] All the structures are designed for 99.975% reflectance at the center wavelength of 1078 nm. The aperiodic multilayer structures are composed of alternating layers of GaAs (76.6 nm), $Al_{0.92}Ga_{0.08}As$ (89.5 nm), and a lattice-matched InGaP etch stop layer (29.6 nm). (c) The reflectance as a function of wavelength in the normal direction for the microresonator mirror pad structures in (a) and (b). The optimized thicknesses of the GaAs and $Al_{0.92}Ga_{0.08}As$ layers are 35.8 nm and 34.7 nm, respectively. Reproduced with permission from Cripe *et al.*, Nature **568**, 7752 (2019). Copyright 2019 Springer Nature Limited.

$Al_{0.92}Ga_{0.08}As$ (with a total thickness of 221.7 nm) under the InGaP buffer layer separately designed as the cantilever for the mirror pad. In other words, the contribution of the cantilever structure to the transmission was neglected when designing the mirror pad. In the microresonator proposed in this paper, the thickness of each $GaAs/Al_{0.92}Ga_{0.08}$ quarter-wave optical pair in the Bragg mirror is kept the same as in Ref. 29. However, the mirror pad and the cantilever of the microresonator are designed together by using the last pair of GaAs and $Al_{0.92}Ga_{0.08}As$ as the cantilever. As such, the thick GaAs layer deposited over the InGaP buffer layer is removed and the thicknesses of the GaAs and $Al_{0.92}Ga_{0.08}As$ layers in the last pair, which is also used for the cantilever, are optimized by our recently developed hybrid optimization algorithm[38] consisting of a micro-genetic global optimization algorithm coupled to a local optimization algorithm.[39] The micro-genetic algorithm, like conventional genetic algorithms, is an iterative optimization procedure which starts with a randomly selected population of potential solutions and evolves toward improved solutions. It has been shown that the micro-genetic algorithm avoids the problem of premature convergence in conventional, large-population genetic algorithms.

The micro-genetic algorithm also shows faster convergence to the near-optimal region, especially when optimizing one-dimensional multilayer structures.[40] The process retains the best structure found and is iteratively repeated. Using this algorithm, the optimized thicknesses for transmission of 250 parts per million (p.p.m.) can be found at the prespecified wavelength of 1078 nm. Our goal is to obtain structures with thinner mirror pad, while the transmission is kept the same as in Ref. 29. Given the optical loss that we have observed in our optomechanical system, larger transmission will allow us to have a more pure measurement and, consequently, a more effective QRPN reduction technique, such as using squeezed light, which is extremely sensitive to optical loss.[41] The $GaAs/Al_{0.92}Ga_{0.08}As$ pair under the InGaP layer not only contributes to the total reflectance of the mirror pad but also supports its weight in the cantilever microresonator. During the optimization with the genetic algorithm, we use a minimum thickness constraint for the thin GaAs/AlGaAs pairs because too thin support layers may lead to a structure that is too fragile. The minimum thickness of GaAs/AlGaAs pairs for the genetic algorithm is fixed to 50 nm based on the mechanical analysis of the microresonator geometries

studied in this paper. Using the genetic algorithm for the proposed microresonator in Fig. 2(b), we found three GaAs/AlGaAs pairs with a transmission of 250 p.p.m.: (1) t_{GaAs} = 50.7 nm, t_{AlGaAs} = 52.1 nm, (2) t_{GaAs} = 41.2 nm, t_{AlGaAs} = 40.9 nm, and (3) t_{GaAs} = 35.8 nm, t_{AlGaAs} = 34.7 nm. Figure 2(c) shows a reflectance of 99.975% corresponding to a transmission of 250 p.p.m. at the center wavelength of 1078 nm at which the structure was optimized for the previously proposed microresonator[29] and for the microresonator proposed in this paper with the thinnest GaAs/AlGaAs pair. The mirror center wavelength is red-shifted to 1078 nm to consider thermorefractive effects upon cooling and, thereby, the ultimate goal of operating these structures at cryogenic (liquid 4He) temperatures.[42] It can be seen that the new microresonator has the same bandwidth as the previous one, while the reflectance at higher and lower frequencies is smaller compared to the previous design.

We model the thermal noise using a FEM model of the microresonator in COMSOL. The FEM model of the cantilever uses the cantilever and mirror geometry, as well as the mechanical properties of the GaAs/AlGaAs cantilever and mirror pad, to compute the modal resonant frequencies. The mechanical modes that are most relevant for the work presented here are the first (fundamental), third (pitch), and fourth modes. We previously demonstrated[43] that the second (yaw) mode is not coupled to our measurement for the beam centered along the microresonator. Structural damping models contain a frequency-independent loss angle φ and for a harmonic oscillator have a displacement amplitude spectral density as follows:[44]

$$x(\omega) = \sqrt{\frac{4k_B T \omega_m^2}{Q_k m \omega \left[\left(\omega_m^2 - \omega^2 \right)^2 + \frac{\omega_m^4}{Q_k} \right]}},\tag{1}$$

where k_B is the Boltzmann constant, T is the temperature, m is the mass, Q = 1/φ is the quality factor, ω = 2π × f, and ω_m is the angular frequency of the mechanical mode. For structural damping, the thermal noise falls off as $1/\omega^{5/2}$ above the mechanical resonance frequency. Viscous damping, on the other hand, is proportional to $1/\omega^2$ above the mechanical resonance.[44]

The optical spring can be considered as a feedback mechanism to form a closed-loop feedback system between the mechanical oscillator and the optical cavity. In this view, the mechanical oscillator, with the mechanical susceptibility χ, transduces a force into a displacement, while the optical cavity, in turn, transduces the displacement back into a radiation pressure force. Radiation pressure is a natural transducer to stabilize such an optical system, and the transmitted power through the cavity is a natural readout of the cavity motion. The SQL sets a limit for conventional continuous displacement measurements and balances the imprecision of the measurement from photon statistics with the unwanted quantum back action (radiation pressure noise). The SQL for the position measurement of a free mass with mass m is calculated based on the mechanical susceptibility χ using $x_{SQL} = \sqrt{2\hbar|\chi|}$.[45]

III. RESULT AND DISCUSSION

Figure 3 shows the spectrum of TN and SQL that is calculated by summing the contribution of each mechanical mode in quadrature for the microresonators in Figs. 2(a) and 2(b) with different geometries at 10 K (the lowest temperature possible to achieve for our equipment). All three microresonators have fundamental resonance frequencies between 100 Hz and 1 kHz, which are in the proper range for designing microresonators with improved sensitivities.[29] Compared to the 55 μm long microresonators (red and blue), the 97 μm long microresonator (black) not only has a larger number of higher-order modes but also the resonances are in the middle of the sub-SQL regime, which is not desirable. However, the short microresonators have a lower
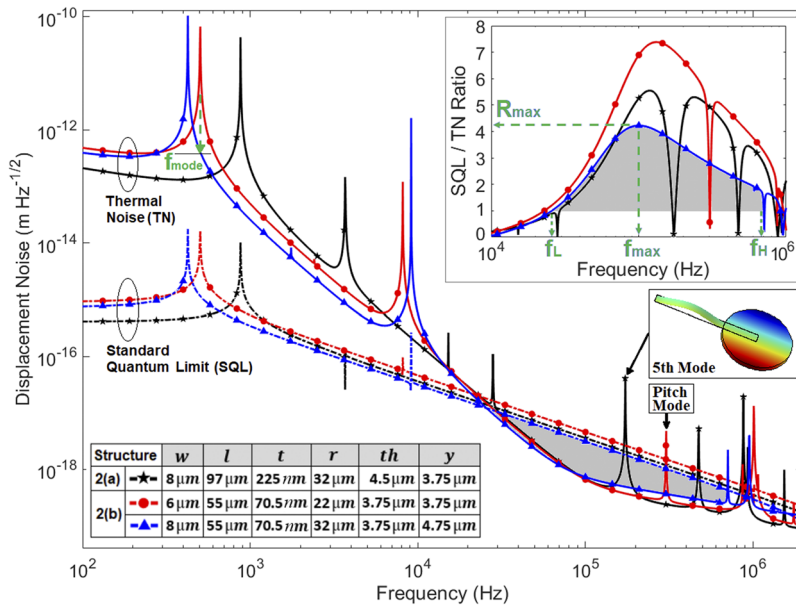

Structure		w	l	t	r	th	y
2(a)	★	8 μm	97 μm	225 nm	32 μm	4.5 μm	3.75 μm
2(b)	●	6 μm	55 μm	70.5 nm	22 μm	3.75 μm	3.75 μm
	▲	8 μm	55 μm	70.5 nm	32 μm	3.75 μm	4.75 μm

FIG. 3. Thermal noise and standard quantum limit as a function of frequency for the microresonators in Fig. 2(a), the microresonator mirror pad design in Ref. 29, and Fig. 2(b) with different geometries. The inset shows the SQL/TN ratio for the microresonators, as well as the definition of the parameters used to study the effects of changing the geometry of the mirror pad and cantilever microresonator on the TN and SQL. The inset also shows the fifth mode of the microresonator in Fig. 2(b) in the BWE region. These parameters include the maximum ratio, R_{MAX}, its frequency, f_{MAX}, the lowest frequency, f_L, and highest frequency, f_H, at which the TN equals to SQL. The two frequencies, f_L and f_H, are used to calculate the frequency bandwidth of TN and SQL equality using BWE = log(f_H) − log(f_L). The geometric parameters of the microresonators are shown in the inset table. Reproduced with permission from Cripe et al., Nature **568**, 7752 (2019). Copyright 2019 Springer Nature Limited.

fundamental mode frequency due to their thin holders of the mirror pad (t = 70.5 nm).

The SQL/TN ratio as a function of frequency for the sub-SQL region of displacement noise is also shown in Fig. 3. Reducing the thermal motion at frequencies away from the resonance enables the sub-SQL regime and serves as a test-bed for very sensitive interferometric experiments. In order to study the sub-SQL region, we define four parameters: (1) the maximum ratio, R_{MAX}, (2) the frequency of maximum ratio, f_{MAX}, (3) the lowest frequency of the sub-SQL region, f_L, at which the TN is equal to the SQL, and (4) the bandwidth of TN and SQL equality (BWE) as $\log(f_H) - \log(f_L)$. Larger R_{MAX} indicates a more secure range of sub-SQL regime and, thereby, better access to test and suppress the QRPN. Expanding the sub-SQL region (e.g., f_{MAX} and f_L) to lower frequencies decreases heat generation from the laser beam in the cryogenic system and, thereby, facilitates the experimental setup. Broadening the sub-SQL range to higher frequencies is promising for future designs of an

unstable filter cavity that operates beyond the frequency limit of 200 kHz in our current experimental setup. We study the effects of changing the geometry of the mirror pad and microresonator cantilever on the sub-SQL region for the proposed microresonator in Fig. 2(b).

A. Length of the microresonator cantilever

Figure 4 shows the effect of varying the length of the microresonator cantilever. The frequency of the fundamental, pitch, and fourth modes as a function of the microresonator cantilever length for the three optimized microresonators is shown in Fig. 4(a). The resonance frequencies of the microresonators decrease as the length of the microresonator cantilever increases. In addition, the fundamental and pitch mode frequencies decrease more rapidly than the one of the fourth mode as the length increases. We observe that the thinner microresonator with $t_{GaAs/AlGaAs}$ = 70.5 nm has the lowest frequencies for the fundamental, pitch, and fourth modes for any
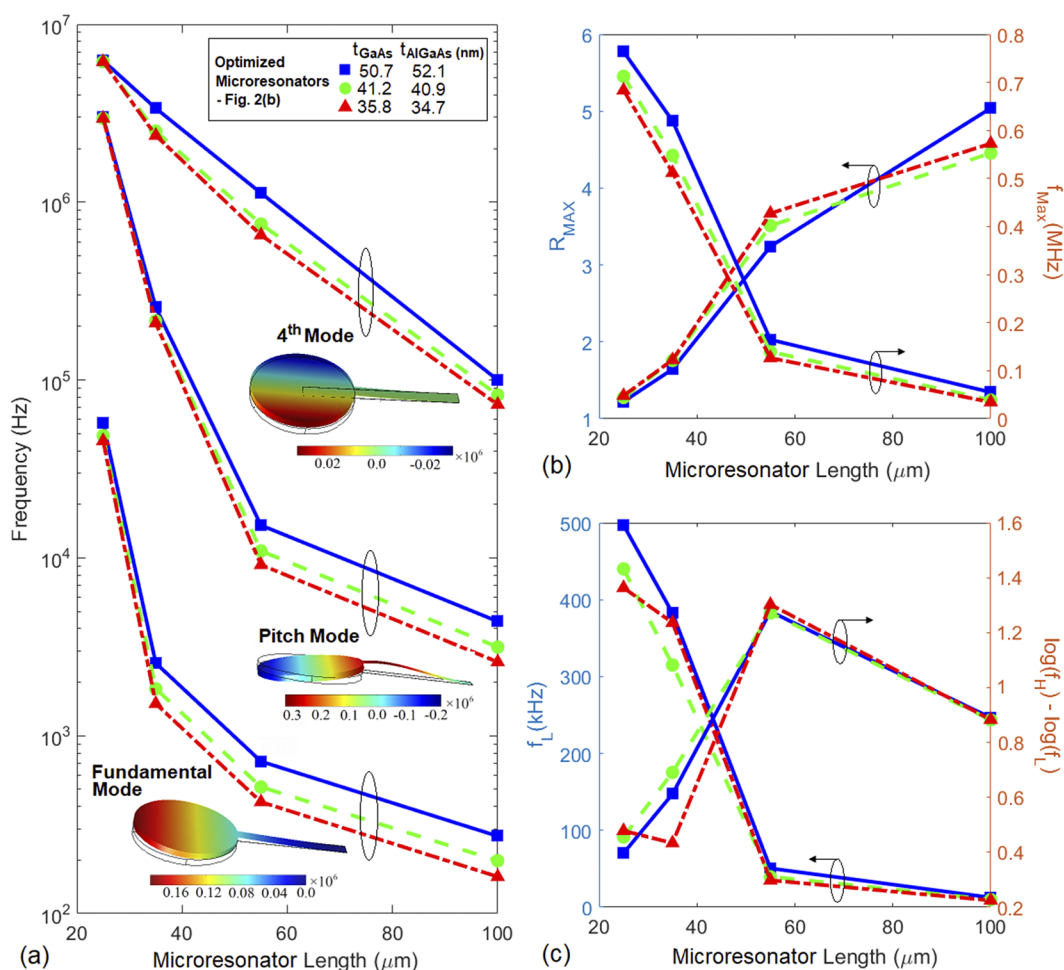

FIG. 4. (a) Resonance frequencies of the fundamental, pitch, and fourth modes, (b) R_{MAX} and f_{MAX}, and (c) f_L and BWE as a function of the microresonator cantilever length for the three microresonators optimized by the genetic algorithm. Results are shown for the fixed parameters of w = 8 μm, r = 32 μm, and y = 3.75 μm. The microresonator mechanical modes of interest are also depicted in the figure.

microresonator cantilever length. However, the dependence of mode frequencies on the thickness of GaAs/AlGaAs pairs increases for longer microresonators. The benefit of using a long cantilever is having a lower fundamental mode frequency and, thereby, lower thermal noise at the frequencies of interest. The two longest microresonators in our study with 55 μm and 100 μm length have a fundamental resonance frequency between 100 Hz and 1 kHz, which, as mentioned above, is the proper range for microresonators with improved sensitivities.[29] On the other hand, the microresonator with 100 μm length has more higher-order modes (e.g., the fourth mode) with frequencies below 200 kHz, which is not a desirable feature.[29]

R_{MAX} increases from ~1.3 to ~4.6 and f_{MAX} decreases from ~700 kHz to ~50 kHz as the length of the microresonator cantilever increases from 25 μm to 100 μm [Fig. 4(b)]. For a length of 55 μm, the thinner microresonator with 70.5 nm thickness of GaAs/AlGaAs has the benefit of both larger R_{MAX} and smaller f_{MAX} and is, thereby, a promising design for a secure range of sub-SQL regime and less heat generation from the laser beam (i.e., broad frequency range shifted to lower frequencies and the displacement noise is well below that of SQL). The lowest frequency, f_L, decreases from ~450 kHz to ~10 kHz by increasing the length of the microresonator cantilever from

25 μm to 100 μm [Fig. 4(c)]. However, the lowest frequency f_L steeply decreases to ~40 kHz as the length decreases to 55 μm, while it only slightly decreases as the length of the microresonator cantilever further increases [Fig. 4(c)]. In other words, f_L is less sensitive to length variations for lengths longer than 55 μm. The BWE increases from 3.4 to 4.3 by increasing the microresonators' cantilever length from 25 μm to 55 μm [Fig. 4(c)]. However, the BWE decreases to 3.9 for a length of 100 μm because the frequency range of SQL/TN >1 decreases due to the shift of higher-order modes to lower frequencies for longer microresonators. Similar to f_L, BWE is less sensitive to length variations for longer microresonator lengths for all three optimized microresonators [Fig. 4(c)]. Thus, for fixed parameters of w = 8 μm, r = 32 μm, and y = 3.75 μm in Fig. 1, we need to choose the microresonator length between 55 μm and l = 100 μm to have a more secure sub-SQL range with the desirable values of low resonance mode frequencies, high R_{MAX}, low f_{MAX}, low f_L, and relatively high BWE.

B. Width of the microresonator cantilever

Figure 5 shows the effect of varying the width of the microresonator cantilever. Decreasing the width of the microresonator
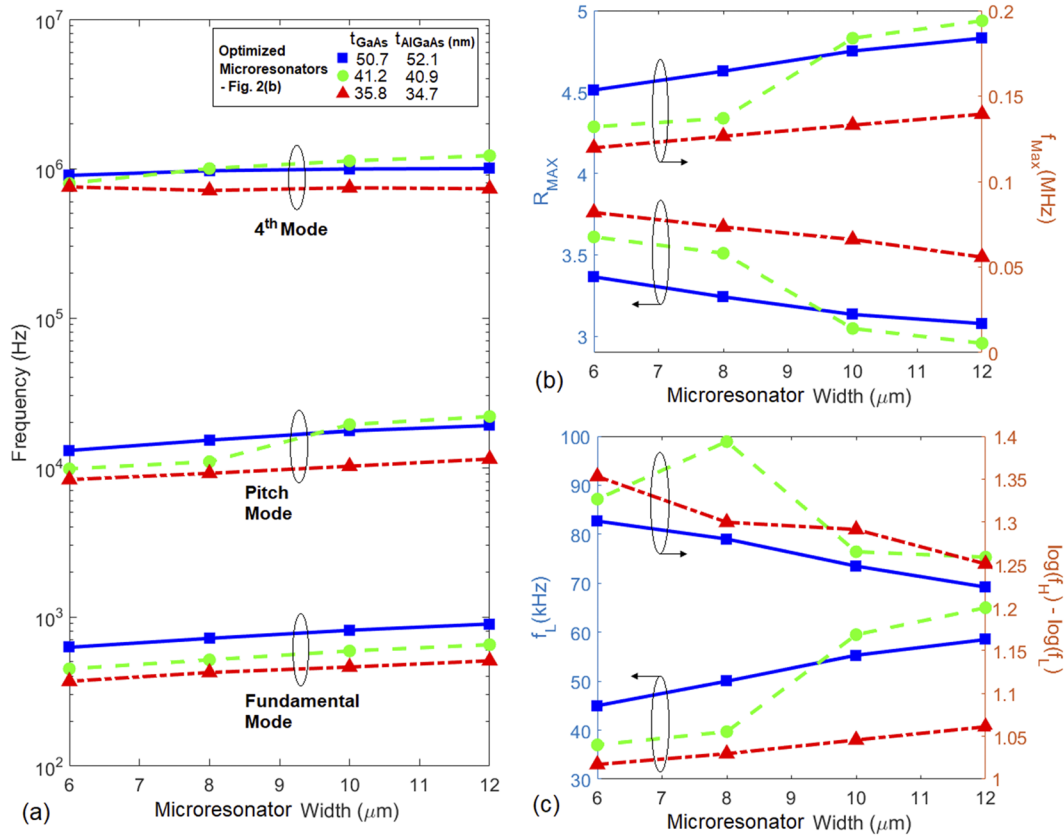

FIG. 5. (a) Resonance frequency of the fundamental, pitch, and fourth modes, (b) R_{MAX} and f_{MAX}, and (c) f_L and BWE as a function of the microresonator width for the three microresonators optimized by genetic algorithm. Results are shown for the fixed parameters of l = 55 μm, r = 32 μm, and y = 3.75 μm.

cantilever from 12 μm to 6 μm lowers the frequency of the fundamental and pitch modes by ~30%, as shown in Fig. 5(a). The frequency of the fourth mode has an insignificant dependence on the width of the microresonator cantilever. The shift of the modes to lower frequencies as the cantilever width is varied is not as significant as the shift caused by changing the length of the cantilever. All three microresonators satisfy the constraint of having the fundamental resonance frequency between 100 Hz and 1 kHz, as well as the higher-order modes above 200 kHz for all cantilever widths considered.[29] The thinner microresonator with $t_{GaAs/AlGaAs}$ = 70.5 nm has lower frequencies of the fundamental, pitch, and fourth modes compared to the other two microresonators. The thinner and narrower microresonator cantilever has a smaller mass that shifts the modes to lower frequencies.

Decreasing the microresonator width from 12 μm to 6 μm increases the R_{MAX} by ~9%, 22%, and 7% for the microresonators with 102.8 nm, 82.1 nm, and 70.5 nm of GaAs/AlGaAs thicknesses, respectively, as shown in Fig. 5(b). For the same change in the microresonator width, the f_{MAX} of the microresonators increases by ~20%, 47%, and 17%, respectively. Similarly, the lowest frequency, f_L, increases by increasing the microresonator widths from

6 μm to 12 μm, as shown in Fig. 5(c). We observe that decreasing the microresonator widths affects the microresonator parameters in the same way as increasing the microresonator lengths. However, the sensitivity to length variations is roughly 10 times larger than the sensitivity to width variations. Decreasing the microresonator widths from 12 μm to 6 μm increases the BWE by 1.8%, 1.4%, and 2.3% for the microresonators with 102.8 nm, 82.1 nm, and 70.5 nm of GaAs/AlGaAs thickness, respectively. Thus, for the fixed parameters of l = 55 μm, r = 32 μm, and y = 3.75 μm in Fig. 1, we have to choose the narrowest microresonator cantilever (w = 6 μm) to have more secure sub-SQL range with the desirable properties of low mode frequencies, high R_{MAX}, low f_{MAX}, low f_L, and relatively high BWE.

C. Size of the microresonator mirror pad

Figure 6 shows the effect of varying the radius of the microresonator mirror pad. Increasing the mirror pad radius from 12 μm to 42 μm decreases the frequency of the fundamental mode by ~60% for all three microresonators considered, as shown in Fig. 6(a). The shift of the fundamental modes to lower frequencies is not as
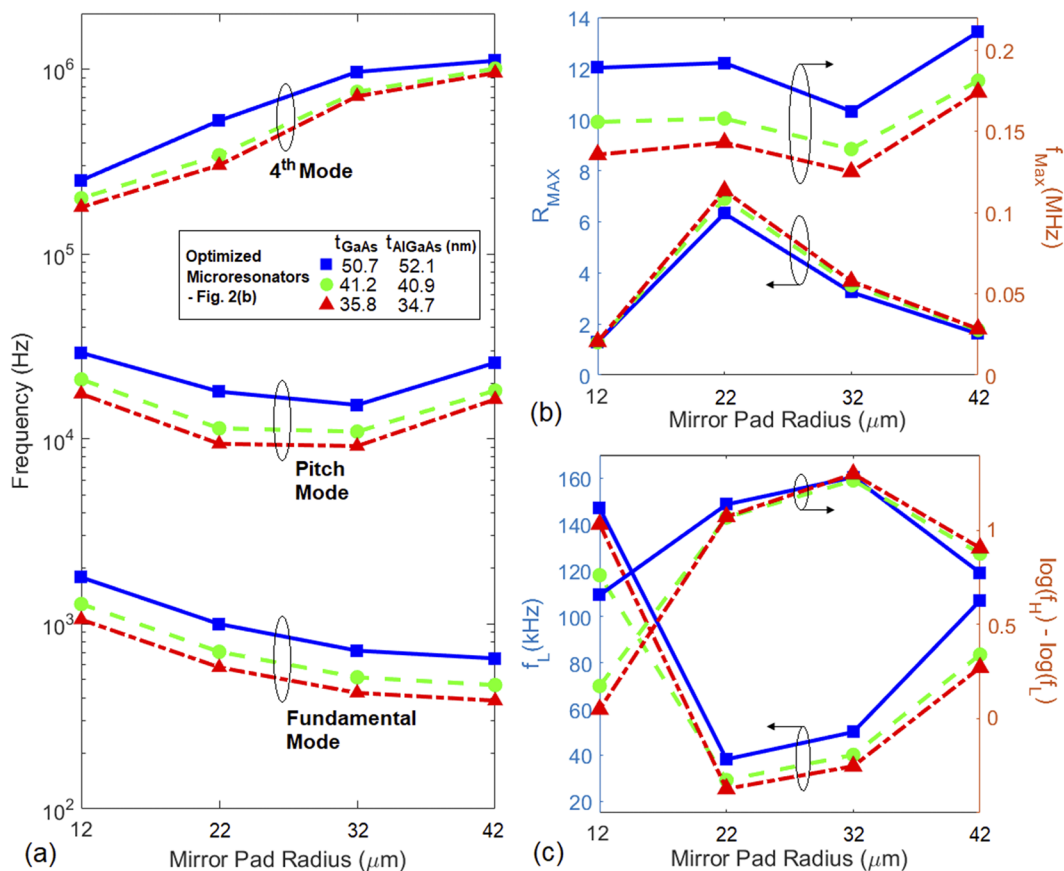

FIG. 6. (a) Resonance frequency of the fundamental, pitch, and fourth modes, (b) R_{MAX} and f_{MAX}, and (c) f_L and BWE as a function of the mirror pad radius for the three microresonators optimized by genetic algorithm. Results are shown for the fixed parameters of l = 55 μm, w = 8 μm, and y = 3.75 μm.

significant as the shift caused by changing the length of the microresonator cantilever but is larger than the shift caused by changing its width. The frequencies of the pitch mode decrease initially and increase to roughly the same frequencies as the mirror pad radius increases to 42 μm. The frequency of the fourth mode increases by a factor of ~5, to a value of ~1 MHz, at a mirror pad radius of 42 μm. Therefore, the increase in mirror radius is beneficial, not only because of the decrease in the frequency of the fundamental mode to below 1 kHz but also because of the increase in the frequency of the fourth and upper modes to above 200 kHz. However, increasing the radius of the mirror pad increases the mass of the mirror and, thereby, decreases the ratio of QRPN to TN.[31]

Increasing the radius of the mirror pad from 12 μm to 22 μm increases R_{MAX} by a factor of ~5. R_{MAX} then decreases to roughly the same value at a mirror pad radius of 42 μm, for all the microresonators, as shown in Fig. 6(b). The f_{MAX} of the microresonators increases by ~11% when changing the radius of the mirror pad from 12 μm to 42 μm. We observe that the sensitivity of f_{MAX} to the radius of the mirror pad is similar to the sensitivity to the microresonator width but smaller than the sensitivity to the microresonator length. Increasing the radius of the mirror pad from 12 μm to 22 μm steeply decreases f_L by a factor of ~2.8, which then increases by a factor of ~1.8 as the radius of the mirror pad increases from 22 μm to 42 μm [Fig. 6(c)]. Increasing the radius of the mirror pad from 12 μm to 32 μm increases the BWE by ~17%, ~35%, and ~40% for the microresonators with 102.8 nm, 82.1 nm, and 70.5 nm GaAs/AlGaAs thicknesses, respectively [Fig. 6(c)]. For the mirror pad with a 42 μm radius, the pitch mode frequency increases and

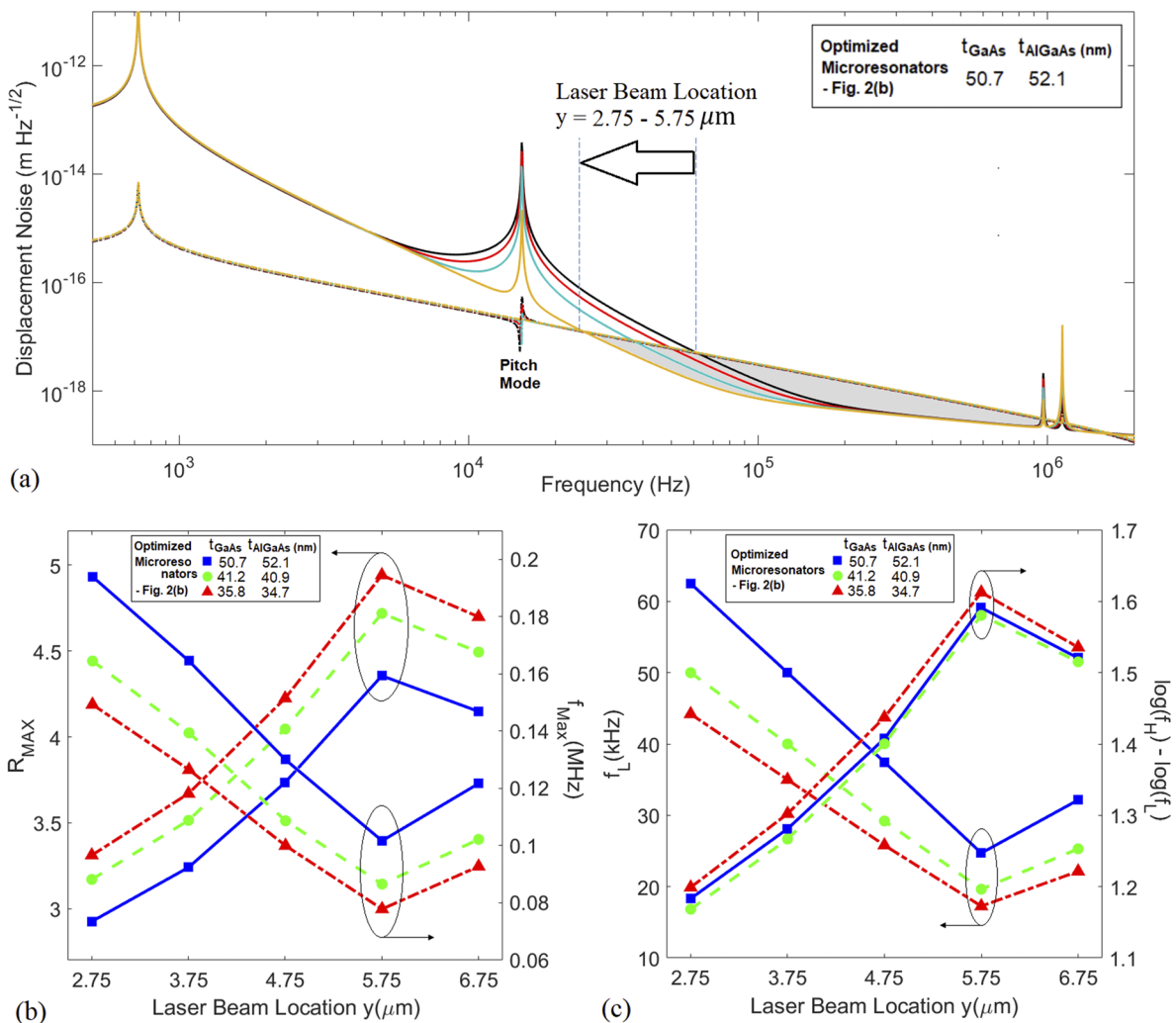**FIG. 7.** (a) Thermal noise and standard quantum limit as a function of frequency for the optimized microresonator in Fig. 2(b) with t_{GaAs} = 50.7 nm and t_{AlGaAs} = 52.1 nm. Moving the location of the laser beam away from the center of the mirror pad, from y = 2.75 μm to 5.75 μm in Fig. 1, sharpens the pitch mode at the fixed frequency of this mode. (b) R_{MAX} and f_{MAX} and (c) f_L and BWE as a function of the laser beam location for the three microresonators optimized by genetic algorithm. Results are shown for the fixed parameters of l = 55 μm, w = 8 μm, and r = 32 μm.

decreases the BWE by ~12% for all three microresonators considered. We observe that the dependence of R_{MAX}, f_{MAX}, f_L, and BWE on the mirror pad radius is not monotonic due to different shifts in the frequency of the fundamental, pitch, and fourth modes as the mirror pad radius is varied. Thus, for the fixed parameters of l = 55 μm, w = 8 μm, and y = 3.75 μm in Fig. 1, the microresonator mirror pad with the 22 μm radius has the highest R_{MAX}, lowest f_L, relatively high BWE and f_{MAX}, and the desirable fundamental mode frequency below 1 kHz to suppress the heat generation from the laser beam.

D. Location of the laser beam on the mirror pad

Figure 7 shows the effect of varying the location of the laser beam, y in Fig. 1, on the microresonator mirror pad. Figure 7(a) shows that there is no change in the frequency of mechanical modes when altering the laser beam location because the laser beam

location is not a geometric parameter of the microresonator. The location of the laser beam, y in Fig. 1, affects the contribution of the pitch mode and changes its sharpness at the fixed frequency of the pitch mode [Fig. 7(a)]. The position-dependent coupling of the optical spring to the pitch mode is analogous to attaching a mechanical spring to different points on the microresonator. We observe that increasing the distance of the laser beam location from the center of the mirror pad sharpens the pitch mode and, thereby, widens the plateau of the sub-SQL region. Figure 7(b) shows that shifting the laser beam location from 2.75 μm to 5.75 μm increases R_{MAX} by ~50% to ~4.95 and decreases f_{MAX} by ~48% to ~78 kHz for the microresonator with the thinnest GaAs/AlGaAs pair and the fixed parameters of l = 55 μm, w = 8 μm, and r = 32 μm. Figure 7(c) shows that f_L decreases by ~60% and the BWE increases by ~10% by shifting the laser beam location from 2.75 μm to 5.75 μm. Thus, for the fixed parameters of l = 55 μm, w = 8 μm, and r = 32 μm in Fig. 1, the microresonator mirror pad with the laser beam location of

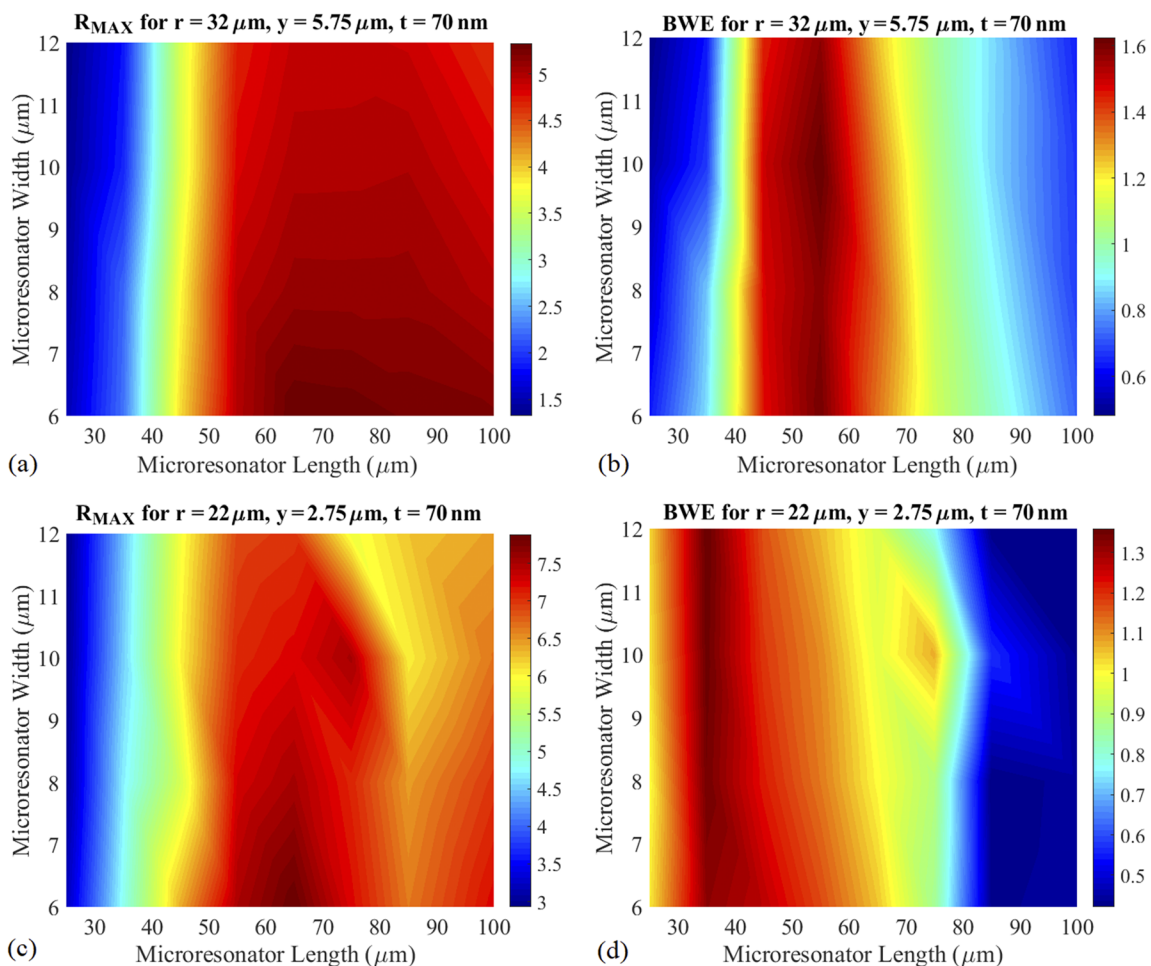**FIG. 8**. (a) R_{MAX} and (b) BWE as a function of the length and width of the thinnest microresonator with $t_{GaAs/AlGaAs}$ = 70 nm for a mirror radius of r = 32 μm and a laser beam location of y = 5.75 μm. (c) R_{MAX} and (d) BWE as a function of the length and width of the thinnest microresonator with $t_{GaAs/AlGaAs}$ = 70 nm, for a mirror radius of r = 22 μm and laser beam location of y = 2.75 μm.

y = 5.75 μm has a more secure sub-SQL range with highest R_{MAX}, lowest f_{MAX}, lowest f_L, and highest BWE.

IV. COMBINED EFFECTS OF GEOMETRIES ON THE SUB-SQL REGION

To study the possible combined effects and interactions among geometric parameters, the BWE and R_{MAX} are depicted as a function of the length and width of the microresonator in Fig. 8. Here, we consider the thinnest microresonator with $t_{GaAs/AlGaAs}$ = 70 nm since the BWE and R_{MAX} of the other optimized microresonators roughly demonstrate the same trend. We calculate the BWE and R_{MAX} as a function of the length and width of the microresonator for two different mirror radii of r = 32 μm [Figs. 8(a) and 8(b)] and r = 22 μm [Figs. 8(c) and 8(d)]. For each radius of the mirror pad, we find the optimal location of the laser beam.

Figure 8(a) shows that R_{MAX} significantly increases from ~1.5 to ~4.5 by changing the length of the microresonator from ~30 μm to ~50 μm, while it is almost independent of the microresonator width for this length range. For all microresonators longer than ~50 μm, R_{MAX} is larger than ~4.5 with a maximum value of ~5.3 for the narrowest microresonator (w = 6 μm) with a length of ~70 μm. Similarly, the BWE significantly increases by increasing the length of the microresonator with a maximum value of ~1.6 for a length close to ~55 μm, as shown in Fig. 8(b). However, unlike R_{MAX}, the BWE decreases by increasing the length of the microresonator because the frequency range of SQL/TN >1 decreases due to the shift of higher-order modes to lower frequencies for longer microresonators.

Figure 8(c) shows that R_{MAX} for the mirror radius of r = 22 μm similarly increases by increasing the length of the microresonator from ~30 μm to ~50 μm. In addition, R_{MAX} is maximized for the narrowest microresonator (w = 6 μm) at the length of ~65 μm, which is similar to the results in Fig. 8(a). However, the decrease in the size of the mirror radius from r = 32 μm to 22 μm leads to an increase in the maximum R_{MAX} from ~5.3 to ~7.8. The larger maximum R_{MAX} of ~7.8 is achieved for a length of ~65 μm. The BWE of the microresonator with the mirror radius of r = 22 μm depicts a behavior similar to that of the microresonator with the mirror radius of r = 32 μm, as shown in Fig. 8(d). However, the microresonator with the smaller radius of mirror pad also needs a shorter cantilever close to ~35 μm to reach the maximum BWE.

Another important conclusion can be obtained by comparing the range of color bars for the R_{MAX} and BWE in Figs. 8(a)–8(d). It can be observed that the microresonator with the larger radius of the mirror pad demonstrates larger BWE at the expense of smaller R_{MAX}. Similarly, the microresonator with the smaller radius of the mirror pad demonstrates larger R_{MAX} at the expense of smaller BWE. In other words, there exists a trade-off between the maximum ratio of TN to SQL (R_{MAX}) and the bandwidth of TN and SQL equality (BWE).

V. SUMMARY AND CONCLUSION

We have designed new microresonators using the microgenetic algorithm and a finite element method model and studied the effect of changing the geometry of the microresonators on the sub-SQL region. We have illustrated the results of our analysis by calculating the spectrum of TN and SQL through summing the contribution of each mechanical mode in quadrature for the microresonators. We find that thinner and longer microresonators have lower frequencies of the fundamental, pitch, and fourth modes and that the sensitivity of the mode frequencies to the microresonator length is more significant than the sensitivity to its width and mirror radius. The proposed microresonators outperform the previous design in the sub-SQL region, demonstrating lower TN under SQL, a broader sub-SQL region, and a sub-SQL region at lower frequencies. We find that the maximum ratio of TN to SQL (R_{MAX}) is increased, its frequency (f_{MAX}) is decreased, and the sub-SQL range (BWE) is increased by increasing the length of the microresonator cantilever, increasing the radius of the mirror pad, decreasing the width of the microresonator cantilever, and shifting the laser beam location from the mirror center. We have studied the possible combined effects and interactions among geometric parameters that reveal a trade-off in finding the optimum values of the R_{MAX} and the BWE. The larger R_{MAX} and smaller f_{MAX} contribute to having a secure range of the sub-SQL regime and suppress the heat generation from the laser beam. The larger BWE extended to higher frequencies shows a promising microresonator for designing an unstable filter cavity that operates beyond the frequency limit of a few hundred kHz in the current experimental setup. Increasing the ratio of SQL to TN and tuning its frequency range serve as a test-bed for not only QRPN measurements but also quantum nondemolition (QND) measurements and macroscopic quantum measurements. This approach promotes the possibility of testing reduction techniques to ultimately obtain a sensitivity below the SQL. The broadband, off-resonance sub-SQL region opens a new regime of precision measurement that is relevant for many practical sensing applications, including large scale interferometric gravitational wave detection.

AUTHOR'S CONTRIBUTIONS

S. Sharifi and Y.M. Banadaki contributed equally to this work.

REFERENCES

[1] A. Einstein, Sitzungsberichte **6**, 844–847 (1915).

[2] A. Abramovici, W. E. Althouse, R. W. Drever, Y. Gursel, S. Kawamura, F. J. Raab, D. Shoemaker, L. Sievers, R. E. Spero, K. S. Thorne et al., Science **256**(5055), 325 (1992).

[3] F. Acernese, M. Agathos, K. Agatsuma, D. Aisa, N. Allemandou, A. Allocca, J. Amarni, P. Astone, G. Balestri, G. Ballardin et al., Classical Quantum Gravity **32**(2), 024001 (2014).

[4] B. P. Abbott, R. Abbott, T. Abbott, M. Abernathy, F. Acernese, K. Ackley, C. Adams, T. Adams, P. Addesso, R. X. Adhikari et al., Phys. Rev. Lett. **116**(6), 061102 (2016).

[5] B. Abbott, R. Abbott, T. Abbott, S. Abraham, F. Acernese, K. Ackley, C. Adams, R. Adhikari, V. Adya, C. Affeldt et al., Phys. Rev. D **99**(12), 122002 (2019).

[6] B. Abbott, R. Abbott, T. Abbott, S. Abraham, F. Acernese, K. Ackley, C. Adams, R. Adhikari, V. Adya, C. Affeldt et al., Astrophys. J. **874**(2), 163 (2019).

[7]B. P. Abbott, R. Abbott, T. Abbott, M. Abernathy, F. Acernese, K. Ackley, C. Adams, T. Adams, P. Addesso, R. Adhikari *et al.*, Classical Quantum Gravity **35**(6), 065009 (2018).

[8]B. P. Abbott, R. Abbott, T. Abbott, S. Abraham, F. Acernese, K. Ackley, C. Adams, R. Adhikari, V. Adya, C. Affeldt *et al.*, Astrophys. J. **875**(2), 122 (2019).

[9]M. Rossi, D. Mason, J. Chen, Y. Tsaturyan, and A. Schliesser, Nature **563**(7729), 53 (2018).

[10]S. Schreppler, N. Spethmann, N. Brahms, T. Botter, M. Barrios, and D. M. Stamper-Kurn, Science **344**(6191), 1486 (2014).

[11]J. Aasi, J. Abadie, B. Abbott, R. Abbott, T. Abbott, M. Abernathy, C. Adams, T. Adams, P. Addesso, R. Adhikari *et al.*, Nat. Photonics **7**(8), 613 (2013).

[12]P. Purdue, Phys. Rev. D **66**(2), 022001 (2001).

[13]A. Buonanno and Y. Chen, Phys. Rev. D **65**(4), 042001 (2002).

[14]D. Mason, J. Chen, M. Rossi, Y. Tsaturyan, and A. Schliesser, Nat. Phys. **15**, 745 (2019).

[15]H. Yu, L. McCuller, M. Tse, L. Barsotti, N. Mavalvala, J. Betzwieser, C. D. Blair, S. E. Dwyer, A. Effler, M. Evans *et al.*, arXiv:2002.01519 (2020).

[16]C. M. Caves, Phys. Rev. Lett. **45**(2), 75 (1980).

[17]M. LaHaye, O. Buu, B. Camarota, and K. Schwab, Science **304**(5667), 74 (2004).

[18]N. Kampel, R. Peterson, R. Fischer, P.-L. Yu, K. Cicak, R. Simmonds, K. Lehnert, and C. Regal, Phys. Rev. X **7**(2), 021008 (2017).

[19]F. Y. Khalili, V. Lazebny, and S. Vyatchanin, Phys. Rev. D **73**(6), 062002 (2006).

[20]V. B. Braginsky, Y. I. Vorontsov, and K. S. Thorne, Science **209**(4456), 547 (1980).

[21]V. B. Braginsky, M. L. Gorodetsky, F. Y. Khalili, and K. S. Thorne, Phys. Rev. D **61**(4), 044002 (2000).

[22]H. J. Kimble, Y. Levin, A. B. Matsko, K. S. Thorne, and S. P. Vyatchanin, Phys. Rev. D **65**(2), 022002 (2001).

[23]J. Harms, Y. Chen, S. Chelkowski, A. Franzen, H. Vahlbruch, K. Danzmann, and R. Schnabel, Phys. Rev. D **68**(4), 042001 (2003).

[24]M. Evans, L. Barsotti, P. Kwee, J. Harms, and H. Miao, Phys. Rev. D **88**(2), 022002 (2013).

[25]E. Oelker, T. Isogai, J. Miller, M. Tse, L. Barsotti, N. Mavalvala, and M. Evans, Phys. Rev. Lett. **116**(4), 041102 (2016).

[26]C. Gräf, B. Barr, A. Bell, F. Campbell, A. Cumming, S. Danilishin, N. Gordon, G. Hammond, J. Hennig, and E. Houston, Classical Quantum Gravity **31**(21), 215009 (2014).

[27]H. Nyquist, Phys. Rev. **32**(1), 110 (1928).

[28]H. B. Callen and T. A. Welton, Phys. Rev. **83**(1), 34 (1951).

[29]J. Cripe, N. Aggarwal, R. Lanza, A. Libson, R. Singh, P. Heu, D. Follman, G. D. Cole, N. Mavalvala, and T. Corbitt, Nature **568**(7752), 364 (2019).

[30]H. Miao, Y. Ma, C. Zhao, and Y. Chen, Phys. Rev. Lett. **115**(21), 211104 (2015).

[31]J. Cripe, N. Aggarwal, R. Singh, R. Lanza, A. Libson, M. J. Yap, G. D. Cole, D. E. McClelland, N. Mavalvala, and T. Corbitt, Phys. Rev. A **97**(1), 013827 (2018).

[32]G. Lovelace, N. Demos, and H. Khan, Classical Quantum Gravity **35**(2), 025017 (2017).

[33]M. Principe, Opt. Express **23**(9), 10938 (2015).

[34]G. D. Cole, W. Zhang, M. J. Martin, J. Ye, and M. Aspelmeyer, Nat. Photonics **7**(8), 644 (2013).

[35]G. D. Cole, W. Zhang, B. J. Bjork, D. Follman, P. Heu, C. Deutsch, L. Sonderhouse, J. Robinson, C. Franz, and A. Alexandrovski, Optica **3**(6), 647 (2016).

[36]G. D. Cole, Proc. SPIE **8458**, 845807 (2012).

[37]M. Longair, Philos. Trans. R. Soc., A **373**(2039), 20140287 (2015).

[38]S. Sharifi, Y. M. Banadaki, V. Nezhad, G. Veronis, and J. P. Dowling, J. Appl. Phys. **124**(23), 233101 (2018).

[39]C. H. Granier, F. O. Afzal, S. G. Lorenzo, M. Reyes, Jr., J. P. Dowling, and G. Veronis, J. Appl. Phys. **116**(24), 243101 (2014).

[40]S. Sharifi, "Applications of stochastic optimization and machine learning in photonic nanostructures and quantum optical systems," Ph.D. dissertation (Louisiana State University, 2020).

[41]J. Cripe, N. Aggarwal, R. Lanza, A. Libson, R. Singh, P. Heu, D. Follman, G. D. Cole, N. Mavalvala, and T. Corbitt, arXiv:1802.10069 (2018).

[42]G. D. Cole, S. Gröblacher, K. Gugler, S. Gigan, and M. Aspelmeyer, Appl. Phys. Lett. **92**(26), 261108 (2008).

[43]J. Cripe, T. Cullen, Y. Chen, P. Heu, D. Follman, G. D. Cole, and T. Corbitt, arXiv:1812.10028 (2018).

[44]P. R. Saulson, Phys. Rev. D **42**(8), 2437 (1990).

[45]P. R. Saulson, *Fundamentals of Interferometric Gravitational Wave Detectors* (World Scientific, 1994).

[46]J. D. Cripe, "Broadband measurement and reduction of quantum radiation pressure noise in the audio band," Ph.D. dissertation (Louisiana State University, 2018).